Received 18 June 2005
Revised 25 September 2006
Accepted 27 September 2006

A hybrid finite difference-finite element method for solving the 3D energy equation in non-isothermal flow past over a tube

A. Arefmanesh
Department of Mechanical Engineering, Islamic Azad University, Tehran, Iran, and
M.A. Alavi
Islamic Azad University, Tehran, Iran

Abstract

Purpose – This paper aims to develop a hybrid finite difference-finite element method and apply it to solve the three-dimensional energy equation in non-isothermal fluid flow past over a tube.

Design/methodology/approach – To implement the hybrid scheme, the tube length is partitioned into uniform segments by choosing grid points along its length, and a plane perpendicular to the tube axis is drawn at each of the points. Subsequently, the Taylor-Galerkin finite element technique is employed to discretize the energy equation in the planes; while the derivatives along the tube are discretized using the finite difference method.

Findings – To demonstrate the validity of the proposed numerical scheme, three-dimensional test cases have been solved using the method. The variation of L^2-norm of the error with mesh refinement shows that the numerical solution converges to the exact solution with mesh refinement. Moreover, comparison of the computational time duration shows that the proposed method is approximately three times faster than the 3D finite element method. In the non-isothermal fluid flow around a tube for $Re = 250$ and $Pr = 0.7$, the results show that the Nusselt number decreases with the increase in the tube length and, for the tube length greater than six times the tube diameter, the average Nusselt number converges to the value for the two-dimensional case.

Originality/value – A hybrid finite difference-finite element method has been developed and applied to solve the 3D transient energy equation for different test cases. The proposed method is faster, and computationally more efficient, compared with the 3D finite element method.

Keywords Finite element analysis, Finite difference methods, Flow, Pipes, Numerical analysis

Paper type Research paper

1. Introduction

Fluid flow over tube banks and their heat transfer analysis have many important design applications for boilers, various kinds of heat exchangers, and chemical and nuclear reactors. In recent years, several two-dimensional experimental as well as numerical studies of the fluid flow over tube banks have been conducted (Launder and Massey, 1978; Chen *et al.*, 1986). However, under certain circumstances, the two-dimensional assumption is not considered accurate enough any more, and a full three-dimensional analysis becomes very attractive. The fin-tube heat exchanger shown in Figure 1 is

International Journal of Numerical Methods for Heat & Fluid Flow
Vol. 18 No. 1, 2008
pp. 50-66

0961-5539
DOI 10.1108/09615530810839741

a typical example. To analyze the heat transfer in this heat exchanger, the three-dimensional Navier-Stokes and energy equations should be solved.

Several three-dimensional numerical simulations of fluid flow and heat transfer have been attempted in recent years. Morton and Tony (1997) solved the three-dimensional Navier-Stokes equations employing a compact mixed-order finite element method. Cairncross *et al.* (2000) and Baer *et al.* (2000), in two consecutive articles, introduced a finite element scheme to predict the free surface flow of incompressible fluids in the three-dimensional cases. More recently, a three-dimensional velocity-vorticity weak form finite element algorithm for solving the Navier-Stokes equations has been developed by Wong and Baker (2002). In a very recent study, Tiwari and Biswas (2003) have conducted a three-dimensional numerical investigation of the fluid flow and heat transfer in a rectangular channel with a built-in circular tube. They used the finite volume method and carried out their calculations for moderate Reynolds numbers.

To circumvent the difficulties corresponding the three-dimensional mesh generation, hybrid numerical schemes have attracted much attention in recent years. Mashayek and Ashgriz (1995) combined the finite element and the finite volume methods in a hybrid scheme to simulate free surface flows and interfaces. Zhang and Dalton (1998) carried out a three-dimensional simulation of a steady approach flow past a circular cylinder at low Reynolds numbers using a hybrid finite difference-spectral element method. Among other hybrid techniques, one can mention a hybrid three-dimensional finite difference-finite element scheme developed by Chen (1998) to analyze seismic wave induced fluid-structure interaction of a vertical cylinder. In a recent paper, Passoni *et al.* (2002) have employed a hybrid spectral element-finite difference method to analyze the hydrodynamic stability theory of linear and nonlinear Navier-Stokes equations.

Although the above-mentioned numerical methods for solving the appropriate three-dimensional problems have proven conventionally implemental, for multi-dimensional complex cases where computational time duration becomes a factor, or in cases where results verifications seem determinative, offering a new approach is prominent.

2. Methodology

In this study, a hybrid finite difference-finite element scheme is developed to solve the transient energy equation in the three-dimensional, non-isothermal fluid flow passing over a circular tube located in a channel. The proposed hybrid scheme is based on discretizing the energy equation by employing the finite difference and the finite element methods along and perpendicular to the tube axis, respectively. To implement the hybrid technique, the tube length is partitioned into m uniform segments by choosing $m + 1$ equally-spaced grid points in the range of $0 < z \leq H$, H being the

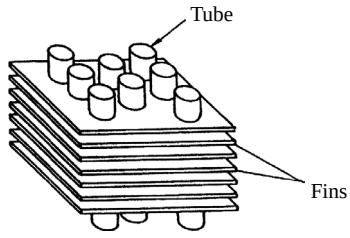

Figure 1.
Schematic diagram of the core region of a fin-tube heat exchanger

tube length, and a plane perpendicular to the tube axis is drawn at each of the grid points. The distance between any two consecutive planes is denoted by Δz (Figure 2). Subsequently, a two-dimensional finite element mesh, consisting of three-noded triangular elements is generated in these planes. Owing to symmetry, the finite element mesh is identical for all the planes. A hybrid three-dimensional mesh is then generated via connecting the nodes of similar triangular elements in different planes by lines parallel to the tube axis (Figure 2).

In order to calculate the temperature distribution, a finite element-based Navier-Stokes equation solver is first utilizied to solve for the flow field. Having obtained the velocity distribution, a two-dimensional Taylor-Galerkin finite element scheme is employed to discretize the energy equation in the planes perpendicular to the tube axis. The derivatives with respect to the z-coordinate, i.e. the derivatives along the tube axis, in the resulting semi-discretized equations are then replaced by the finite difference quotients, establishing the hybrid finite difference-finite element scheme.

The transient continuity, momentum, and energy equations for the three-dimensional, incompressible, laminar flow of a Newtonian fluid in a dimensionless form are, respectively, given by:

$$\nabla.\mathbf{V} = 0 \tag{1}$$

$$\frac{\mathrm{D}\mathbf{V}}{\mathrm{D}t} = -\nabla P + \frac{1}{Re}\nabla^2\mathbf{V} \tag{2}$$

$$\frac{\mathrm{D}\theta}{\mathrm{D}t} = \frac{1}{Pe}\nabla^2\theta \tag{3}$$

where, $\mathbf{V} = (u, v, w)$ is the dimensionless velocity vector, t is the dimensionless time, P is the dimensionless pressure, Re is the Reynolds number, θ is the dimensionless temperature, and Pe is the Peclet number. The dimensionless variable are difined as follows:

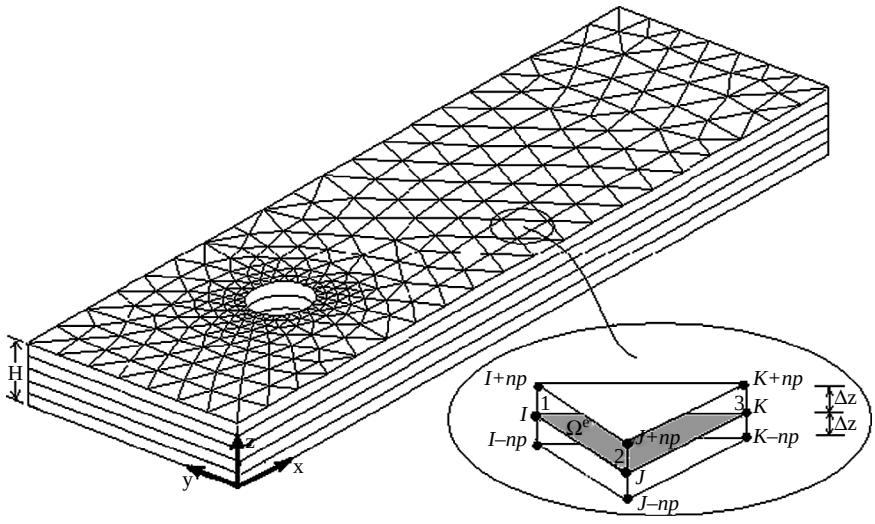

Figure 2.
A hybrid 3D mesh generated in the computational domain using triangular elements

$$Pe = \frac{\rho C_p U_\infty D}{k}, \quad Re = \frac{\rho U_\infty D}{\mu}, \quad \mathbf{X} = \frac{\overline{\mathbf{X}}}{D}, \quad P = \frac{\overline{P}}{\rho U_\infty^2}, \quad t = \frac{\bar{t} U_\infty}{D},$$
$$\theta = \frac{T - T_\infty}{T_w - T_\infty}, \quad \mathbf{V} = \frac{\overline{\mathbf{V}}}{U_\infty} \tag{4}$$

where, ρ is the fluid density, C_p is its specific heat, U_∞ is the free-stream velocity, D is the tube diameter, k is the fluid thermal conductivity, μ is its viscosity, $\mathbf{X}$ is the dimensionless coordinate vector, $\overline{\mathbf{X}}$ is the coordinate vector, $\overline{P}$ is the pressure, $\bar{t}$ is the time, T is the temperature, T_∞ is the free-stream temperature, T_w is the wall temperature, and $\overline{\mathbf{V}}$ is the velocity vector.

The computational domain, and the boundary conditions for the problem are shown in Figure 3. The tube is confined between the top and bottom walls with H being the distance between them. The side-walls are planes of symmetry between the tubes in a tube bundle. The distance between these walls, B, is four times the tube diameter, D. The tube axis is located at a distance equal to 3D from the input plane, i.e. from the y-z plane. The length of the computational domain in the x-direction, L, (which should be long enough for the fully-developed boundary conditions to be applicable at the outlet plane) is set to be equal to 12D. This length has been selected in accordance with the published results in the work done by Tezduyar and Shih (1991).

In this work, the no-slip assumption, and the boundary conditions $T = T_w$ are imposed at the tube surface and along the top and bottom walls. At the input plane, the velocity and the temperature are set equal to the free-stream velocity, U_∞, and the free-stream temperature, T_∞, respectively. At the outlet plane, which is located far enough downstream from the tube for the flow to be fully-developed, the derivatives of velocity and temperature in the x-direction are considered to be zero. Owing to symmetry, the y-derivatives of all the dependent variables and also the y-component of the velocity vector are set equal to zero along the side-walls. Moreover, a reference value of zero is prescribed for the pressure at the outlet plane. The initial conditions are:

$$\mathbf{V}(\mathbf{X}, 0) = 0 \tag{5}$$

$$\theta(\mathbf{X}, 0) = 0. \tag{6}$$

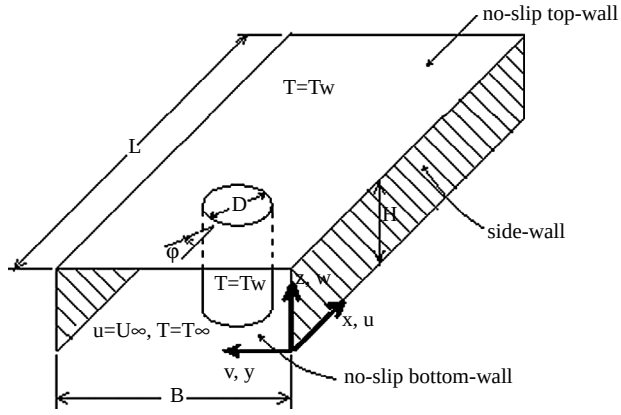

Figure 3.
Domain and boundary conditions for the non-isothermal flow past over the tube

The mathematical model of the problem is expressed by the coupled system of equations (1)-(3), the initial conditions (5) and (6), and the aforementioned boundary conditions shown in Figure 3.

3. Numerical modeling

Before solving the energy equation, the flow field has to be established. A finite element-based Navier-Stokes equation solver is employed for this purpose. A mesh consisting of four-noded tetrahedral elements is used to solve for the flow field. The velocity field is approximated within four-noded tetrahedral elements using linear shape functions, and the pressure is considered to be piecewise constant within the elements (Heinrish and Pepper, 1999). Substituting these approximations into the Petrov-Galerkin weighted residual weak form of the Navier-Stokes equations and discretizing the time derivatives result in a coupled system of nonlinear algebraic equations for the unknown nodal pressure and velocity components (Heinrish and Pepper, 1999; Brooks and Hughes, 1982). The solution of the system of equations yields the pressure and velocity distributions in the computational domain at each time step.

The equation of energy, equation (3), is discretized using the proposed hybrid method. In this method, a two-dimensional finite element technique with three-noded triangular elements is employed to discretize the equation in the planes perpendicular to the tube axis, i.e. *x-y* planes (Figure 2). Subsequently, the resulting semi-discretized ordinary differential equations are discretized using the finite difference method along the tube axis, i.e. in the *z*-direction. Since, utilizing the Galerkin finite element method in the *x-y* planes yields oscillatory solutions for high Peclet numbers, an upwinding scheme is employed to obtain stable solutions. In this study, the Taylor-Galerkin technique, which is suitable for the transient cases, is utilized for this purpose. To implement this technique, a second-order-accurate truncated Taylor series of temperature with respect to time in the dimensionless form is written as:

$$\theta^{n+1} = \theta^n + \Delta t \frac{\partial \theta^n}{\partial t} + \frac{\Delta t^2}{2} \frac{\partial^2 \theta^n}{\partial t^2} \tag{7}$$

where n and $n+1$ represent two consecutive time steps. The first and second derivatives of temperature with respect to time in the above equation are written using equation (3) as:

$$\frac{\partial \theta^n}{\partial t} = -\mathbf{V}.\nabla\theta^n + \frac{1}{Pe}\nabla^2\theta^n \tag{8a}$$

$$\frac{\partial^2 \theta^n}{\partial t^2} = -\frac{\partial V^n}{\partial t}.\nabla\theta^n - (\mathbf{V}^n.\nabla)\frac{\partial \theta^n}{\partial t} + \frac{1}{Pe}\nabla^2\left(\frac{\partial \theta^n}{\partial t}\right). \tag{8b}$$

Substituting expressions (8a) and (8b) into equation (7), and replacing $(\partial\theta^n/\partial t)$ by $((\theta^{n+1} - \theta^n)/\Delta t)$ in the resulting equation, yield the following time-discretized form of the energy equation (Usmani *et al.*,1992; Arefmanesh and Afkhami, 2001):

$$\left(\frac{1}{\Delta t} - \frac{1}{2Pe}\nabla^2\right)\theta^{n+1} = \left[\frac{1}{\Delta t} + \frac{1}{2Pe}\nabla^2 - \mathbf{V}^{n+(1/2)}.\nabla + \frac{\Delta t}{2}(\mathbf{V}^n.\nabla)(\mathbf{V}^n.\nabla)\right]\theta^n. \tag{9}$$

Subsequently, the Galerkin finite element method is employed to discretize equation (9) in the *x-y* planes. For this purpose, the dimensionless temperature is approximated within a typical three-noded triangular element, Ω^e, of the two-dimensional mesh (Figure 2) using the following linear interpolation:

$$\bar{\theta}^{(e)}(x,y,z,t) = \sum_{i=1}^{3} N_i^{(e)}(x,y)\theta_i^{(e)}(z,t) \tag{10}$$

where, $\bar{\theta}^{(e)}$ is the linear approximation of the dimensionless temperature, and $N_i^{(e)}$ and $\theta_i^{(e)}$, for $i = 1\text{-}3$, are the usual linear shape functions (Heinrish and Pepper, 1999) and the nodal values of the dimensionless temperature, respectively. The Galerkin weighted residual formulation of the problem is then obtained by multiplying equation (9) with the shape functions and setting the integral of the resulting expressions over the element equal to zero as shown in the following equation:

$$\int_{\Omega^e} \left\{ \left(\frac{1}{\Delta t} - \frac{1}{2Pe}\nabla^2\right)\theta^{n+1} - \left[\frac{1}{\Delta t} + \frac{1}{2Pe}\nabla^2 - \mathbf{V}^{n+(1/2)}.\nabla + \frac{\Delta t}{2}(\mathbf{V}^n.\nabla)(\mathbf{V}^n.\nabla)\right]\theta^n \right\} N_j \mathrm{d}x\mathrm{d}y = 0, \quad \text{for } j = 1-3 \tag{11}$$

Using the Gauss's theorem, equation (11) can be written as:

$$\begin{aligned}
&\int_{\Omega^e} \left\{ \left(\frac{\theta^{n+1}N_j}{\Delta t} + \frac{1}{2Pe}\left(\frac{\partial\theta^{n+1}}{\partial x}\frac{\partial}{\partial x} + \frac{\partial\theta^{n+1}}{\partial y}\frac{\partial}{\partial y} - \frac{\partial^2\theta^{n+1}}{\partial z^2}\right)N_j\right) \right. \\
&- \left(\frac{\theta^n N_j}{\Delta t} - \frac{1}{2Pe}\left(\frac{\partial\theta^n}{\partial x}\frac{\partial}{\partial x} + \frac{\partial\theta^n}{\partial y}\frac{\partial}{\partial y} - \frac{\partial^2\theta^n}{\partial z^2}\right)N_j\right) \\
&\frac{\Delta t}{2}\left(\left(u^2\frac{\partial\theta^n}{\partial x}\frac{\partial}{\partial x} + v^2\frac{\partial\theta^n}{\partial y}\frac{\partial}{\partial y} - w^2\frac{\partial^2\theta^n}{\partial z^2}\right)N_j\right) \\
&+ \left(\left(u^{n+(1/2)}\frac{\partial\theta^n}{\partial x} + v^{n+(1/2)}\frac{\partial\theta^n}{\partial y} + w^{n+(1/2)}\frac{\partial\theta^n}{\partial z}\right)N_j\right) \\
&\left. + \frac{\Delta t}{2}\left(\left(uv\frac{\partial\theta^n}{\partial x}\frac{\partial}{\partial y} + uv\frac{\partial\theta^n}{\partial y}\frac{\partial}{\partial x} - 2uw\frac{\partial\theta^n}{\partial z}\frac{\partial}{\partial x} - 2vw\frac{\partial\theta^n}{\partial z}\frac{\partial}{\partial y}\right)N_j\right)\right\} \mathrm{d}x\mathrm{d}y = 0,
\end{aligned} \tag{12}$$

for $j = 1-3$.

Since, the boundary conditions for equation (3) are of either essential or zero-derivative types, no boundary integral appears in equation (12).

Substituting the linear approximations for θ^n and θ^{n+1} from equation (10) into equation (12) yields the following system of ordinary differential equations for the typical element:

$$\left(\frac{\mathbf{M}^{(e)}}{\Delta t}+\frac{\mathbf{K}_{\mathrm{d}}^{(e)}}{2Pe}\right)\{\theta^{(e)}\}^{n+1}-\frac{\mathbf{M}^{(e)}}{2Pe}\frac{\mathrm{d}^2\{\theta^{(e)}\}^{n+1}}{\mathrm{d}z^2}=\left(\frac{\mathbf{M}^{(e)}}{\Delta t}-\frac{\mathbf{K}_{\mathrm{d}}^{(e)}}{2Pe}-(\mathbf{K}_{\mathrm{a}}^{(e)}+\mathbf{K}_{\mathrm{bd}}^{(e)})\right)\{\theta^{(e)}\}$$
$$+\left(\frac{1}{2Pe}+\frac{\Delta t}{2}w^2\right)\mathbf{M}^{(e)}\frac{\mathrm{d}^2\{\theta^{(e)}\}^{nn}}{\mathrm{d}z^2}-(w^{n+(1/2)}\mathbf{M}^{(e)}-w\Delta t\mathbf{K}_{\mathrm{a}}^{(e)})\frac{\mathrm{d}\{\theta^{(e)}\}^{n}}{\mathrm{d}z} \tag{13}$$

where, $\mathbf{M}^{(e)}$, $\mathbf{K}_{\mathrm{d}}^{(e)}$, $\mathbf{K}_{\mathrm{a}}^{(e)}$, and $\mathbf{K}_{\mathrm{bd}}^{(e)}$ are the mass, diffusion, advection, and balancing diffusion matrices for the element, respectively, and $\{\theta^{(e)}\}$ with the elements $\theta_i^{(e)}$, for $i=1-3$, is the vector of nodal unknowns. The elements of the above matrices, in terms of the local node numbers are given by:

$$\mathbf{M}_{ij}^{(e)}=\int_{\Omega^e}N_i^{(e)}N_j^{(e)}\mathrm{d}x\mathrm{d}y \tag{14a}$$

$$\mathbf{K}_{\mathrm{d}_{ij}}^{(e)}=\int_{\Omega^e}(N_{i,x}^{(e)}N_{j,x}^{(e)}+N_{i,y}^{(e)}N_{j,y}^{(e)})\mathrm{d}x\mathrm{d}y \tag{14b}$$

$$\mathbf{K}_{\mathrm{a}_{ij}}^{(e)}=\int_{\Omega^e}(u^{n+(1/2)}N_{j,x}^{(e)}N_i^{(e)}+v^{n+(1/2)}N_{j,y}^{(e)}N_i^{(e)})\mathrm{d}x\mathrm{d}y \tag{14c}$$

$$\mathbf{K}_{\mathrm{bd}_{ij}}^{(e)}=\frac{\Delta t}{2}\int_{\Omega^e}(u^2N_{i,x}^{(e)}N_{j,x}^{(e)}+v^2N_{i,y}^{(e)}N_{j,y}^{(e)}+uvN_{i,x}^{(e)}N_{j,y}^{(e)}+uvN_{i,y}^{(e)}N_{j,x}^{(e)})\,\mathrm{d}x\,\mathrm{d}y, \tag{14d}$$

for $i,j=1-3$.

The next step in the numerical solution of the energy equation is to discretize the system of ordinary differential equations for the element (equation (13)) in the z-direction. The finite difference method is employed for this purpose. To implement the method, the vector of nodal unknowns for the element is expressed in terms of the global node numbers as:

$$\{\theta^{(e)}\}^{\ell}=\left\{\begin{array}{c}\theta_I\\ \theta_J\\ \theta_K\end{array}\right\}^{\ell},\quad \text{for } \ell=n,n+1 \tag{15}$$

where I, J, and K are the global node numbers of the element (Figure 2). The difference quotients for the first and second derivatives of the dimensionless temperature with respect to the z-coordinate in equation (13) can then be written in terms of the global node numbers as:

$$\frac{\mathrm{d}\theta_i^{\ell}}{\mathrm{d}z}=\frac{\theta_{i+\mathrm{np}}^{\ell}-\theta_{i-\mathrm{np}}^{\ell}}{2\Delta z},\quad i=I,J,K \tag{16a}$$

$$\frac{\mathrm{d}^2\theta_i^{\ell}}{\mathrm{d}z^2}=\frac{\theta_{i-\mathrm{np}}^{\ell}-2\theta_i^{\ell}+\theta_{i+\mathrm{np}}^{\ell}}{\Delta z^2},\quad \ell=n,n+1 \tag{16b}$$

where, np is the total number of nodes in each of the planes perpendicular to the tube axis, and Δz is the distance between any two consecutive planes (Figure 2).

Substituting expressions (16a) and (16b) into equation (13) yields, the following fully-discretized form of the energy equation for the element:

$$\begin{aligned}\left(\frac{\mathbf{M}^{(e)}}{\Delta t}+\frac{\mathbf{K}_{\mathrm{d}}^{(e)}}{2Pe}\right)\{\theta_i\}^{n+1}-\frac{\mathbf{M}^{(e)}}{2Pe}\,\frac{\{\theta_{i-\mathrm{np}}-2\theta_i+\theta_{i+\mathrm{np}}\}^{n+1}}{\Delta z^2}\\ =\left(\frac{\mathbf{M}^{(e)}}{\Delta t}-\frac{\mathbf{K}_{\mathrm{d}}^{(e)}}{2Pe}-(\mathbf{K}_a^{(e)}+\mathbf{K}_{\mathrm{bd}}^{(e)})\right)\{\theta_i\}^{n}\\ +\left(\frac{1}{2Pe}+\frac{\Delta t\,w^2}{2}\right)\mathbf{M}^{(e)}\,\frac{\{\theta_{i-\mathrm{np}}-2\theta_i+\theta_{i+\mathrm{np}}\}^{n}}{\Delta z^2}\\ -(w^{n+(1/2)}\mathbf{M}^{(e)}-w\Delta t\mathbf{K}_{\mathrm{a}}^{(e)})\,\frac{\{\theta_{i+\mathrm{np}}-\theta_{i-\mathrm{np}}\}^{n}}{2\Delta z}\end{aligned} \tag{17}$$

where, $i = I, J, K$, and all the matrices are written in terms of the global node numbers.

Subsequently, the algebraic equation (17) are assembled for the elements of the hybrid mesh. The essential boundary conditions for the temperature are then applied. The resulting system of algebraic equations is solved and the nodal values of temperature are obtained at each time step. Having obtained the temperature distribution, the local and the average Nusselt numbers are calculated from the following relations, respectively:

$$Nu=-\left.\frac{\partial\theta}{\partial n}\right|_{\mathrm{wall}}=-\sum_{j=1}^{3}\frac{\partial N_j}{\partial n}\,\theta_j \tag{18}$$

$$\overline{N}u=\frac{1}{2\pi}\int_0^{2\pi}Nu\mathrm{d}\varphi \tag{19}$$

where, $\partial()/\partial n$ is the normal derivative. Next, the velocity and the temperature distributions for the ensuing time step are calculated in a similar manner. This procedure is continued until steady-state conditions are developed.

4. Results and discussions

A hybrid finite difference-finite element scheme has been proposed and applied to the solution of the energy equation in the three-dimensional, transient, and non-isothermal fluid flow past over a circular tube. To discretize the energy equation, the proposed hybrid scheme employes the two-dimensional finite element method in the x-y planes, while the derivatives along the z-direction are approximated with the finite difference quotients. The Taylor-Galerkin method has been utilized in order to stabilize the discretization scheme for high Peclet numbers. The following discussions are identified using $D = 0.01$ m, $Re = 250$, $Pr = 0.7$, $T_{\mathrm{w}} = 400$ K and $T_\infty = 300$ K as a test case.

4.1 The method validity

To demonstrate the validity of the numerical implementation, the following three-dimensional, transient, convection-diffusion equation in a unit cube is considered:

$$\frac{\partial T}{\partial t}+a\frac{\partial T}{\partial x}+b\frac{\partial T}{\partial y}+c\frac{\partial T}{\partial z}=\mu\left(\frac{\partial^2 T}{\partial x^2}+\frac{\partial^2 T}{\partial y^2}+\frac{\partial^2 T}{\partial z^2}\right) \tag{20}$$

The exact, steady-state solution of equation (20) for the following boundary conditions:

$$T(0,y,z,t)=\left\{\frac{1-\exp[(y-1)b/\mu]}{1-\exp(-b/\mu)}\right\}\left\{\frac{1-\exp[(z-1)c/\mu]}{1-\exp(-c/\mu)}\right\},\quad T(1,y,z,t)=0 \tag{21a}$$

$$T(x,0,z,t)=\left\{\frac{1-\exp[(x-1)a/\mu]}{1-\exp(-a/\mu)}\right\}\left\{\frac{1-\exp[(z-1)c/\mu]}{1-\exp(-c/\mu)}\right\},\quad T(x,1,z,t)=0 \tag{21b}$$

$$T(x,y,0,t)=\left\{\frac{1-\exp[(x-1)a/\mu]}{1-\exp(-a/\mu)}\right\}\left\{\frac{1-\exp[(y-1)b/\mu]}{1-\exp(-b/\mu)}\right\},\quad T(x,y,1,t)=0 \tag{21c}$$

and the initial condition:

$$T(x,y,z,0)=0 \tag{22}$$

is given by:

$$T_a(x,y,z,t)=\left\{\frac{1-\exp[(x-1)a/\mu]}{1-\exp(-a/\mu)}\right\}\left\{\frac{1-\exp[(y-1)b/\mu]}{1-\exp(-b/\mu)}\right\}\times\left\{\frac{1-\exp[(z-1)c/\mu]}{1-\exp(-c/\mu)}\right\}. \tag{23}$$

Equation (20) for the specified boundary and initial conditions for a, b, c and μ equal to unity has been solved by the proposed hybrid method using three different meshes as discussed earlier. Figure 4 shows the variation of L^2-norm of the error:

$$\|e\|_o=\left[\int_\Omega (T_a-T)^2 d\Omega\right]^{1/2},\quad \Omega=\{0\le x,y,z\le 1\},$$

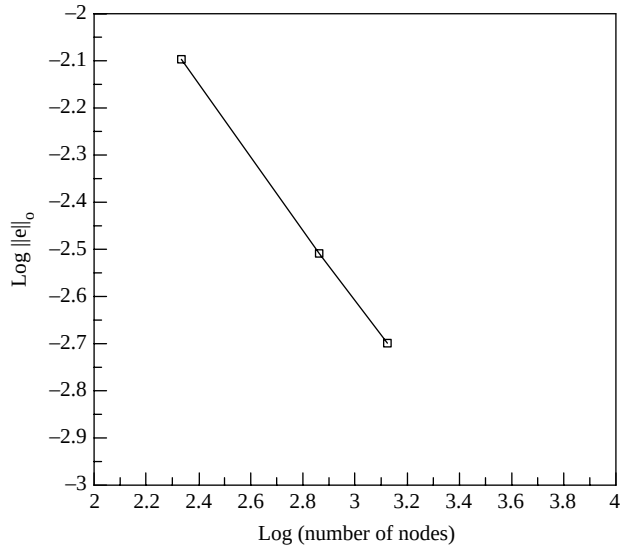

Figure 4.
Variation of the L^2-norm of the error with respect to the number of nodes for equation (20)

versus the number of nodes between the exact and the numerical solutions of equation (20) for the steady-state case. Convergence of the numerical solution to the exact solution of equation (20) with refining the hybrid mesh is apparent in the figure. These results demonstrate the capability of the proposed hybrid method for solving three-dimensional problems.

To compare the time duration for the proposed hybrid scheme with that of the three-dimensional finite element method, consider the finest hybrid mesh used for the results shown in Figure 4 with 1,331 nodes. The computational time for solving equation (20) for 100 time steps using the hybrid scheme for this mesh is 2,800 s using an Intel® – Pentium® 4. This, versus 8,400 s for the three-dimensional finite element method using four-noded tetrahedral elements for the same time step and nodes performed with the same computer.

The principal reason for the lower computational time of the hybrid scheme is its lower nodal connectivity compared to the three-dimensional finite element method. For both the cases, the computer codes employed were unoptimized research versions, and it is expected that optimization would improve the time efficiency.

4.2 Mesh independent study

Before settling with the final mesh, mesh independent studies have been performed for solving the energy equation in non-isothermal flow passing over the tube. In this respect, four different meshes with 2,816, 4,488, 7,216, and 8,107 nodes have been employed to solve the energy equation. Owing to large gradients close to the tube surface, the meshes have been refined in this region. In all the four cases, L/D was chosen to be equal to 12.

The solution of the energy equation is expressed in terms of the Nusselt number. Figure 5 shows the variation of the average Nusselt number with respect to the number of nodes. Convergence of the average Nusselt number to a unique value with mesh refinement is clearly demonstrated in this figure; therefore, showing that for the mesh with 7,216 nodes or finer ones the results are mesh independent. Based on these observations,

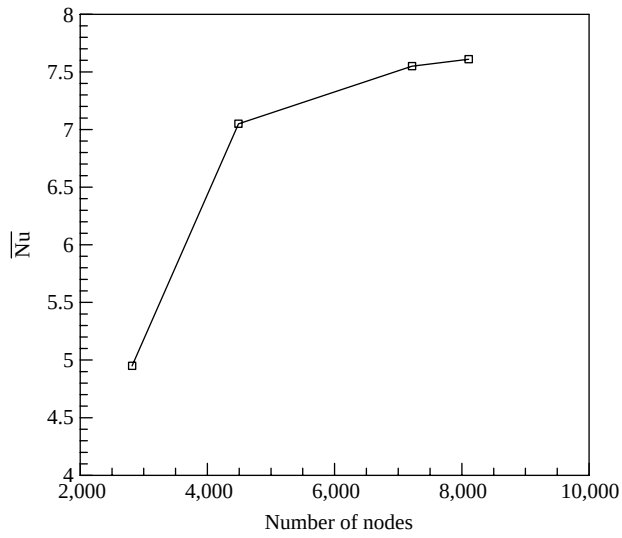

Figure 5.
Variation of the average Nusselt number with mesh refinement for $L/D = 12$

the mesh with 7,216 nodes (consisting of 1,164 triangular elements in each x-y plane, and 36 divisions along the tube) is chosen for the heat transfer results to be presented in the rest of this section.

4.3 Effects of the domain size

As stated previously, the fully-developed boundary conditions are applied at the outlet plane. However, the domain length should be sufficiently large for these boundary conditions to be applicable. To investigate the effect of domain size on the results, numerical experiments have been carried out for different values of L/D.

Figure 6 shows the variation of the average Nusselt number with respect to the domain length. Here, an effort was made to preserve the same mesh density for all the cases presented in this figure. It is observed from the results that the average Nusselt number tends to approach a constant value for $L/D \geq 12$. Therefore, increasing the length beyond 12 D does not have any tangible effects on the results. Hence, the domain length has been chosen to be 12 times of the tube diameter in this study.

4.4 Heat transfer results

Having investigated some different aspects of the proposed hybrid scheme, the results obtained by solving the energy equation for non-isothermal flow past over the tube using this scheme are presented here for the domain length of 12 D, the mesh with 7,216 nodes, and a time step of 0.001. Having obtained the temperature distribution, the local and the average Nusselt numbers are evaluated from relations (18) and (19), respectively.

Figures 7-9 show the distribution of local Nusselt number around the tube for some of the planes perpendicular to the tube axis at different times. It is observed from these results that the local Nusselt number is symmetric with respect to the plane perpendicular to the y-axis which passes through the tube centerline. Moreover, the local Nusselt number is also symmetric with respect to the mid-plane perpendicular to

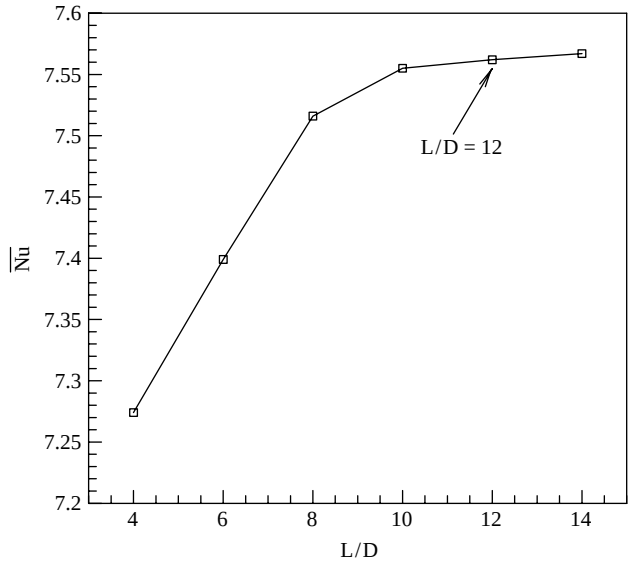

Figure 6.
Variation of the average Nusselt number for flow past over the tube with respect to the domain length

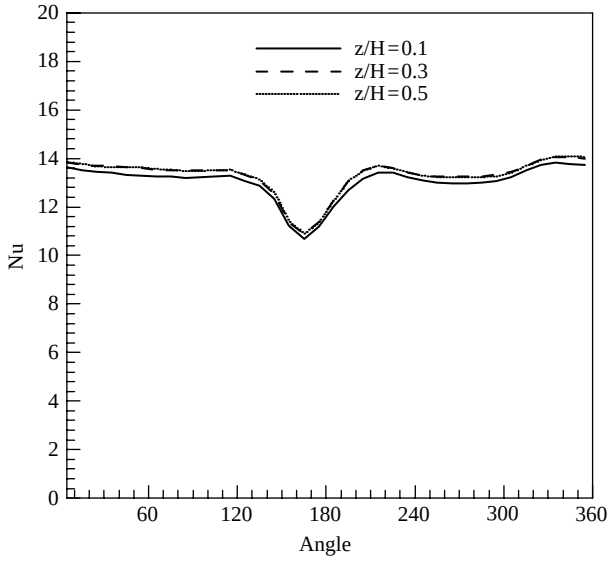

Figure 7.
Local Nusselt number around the tube at $t = 0.1$

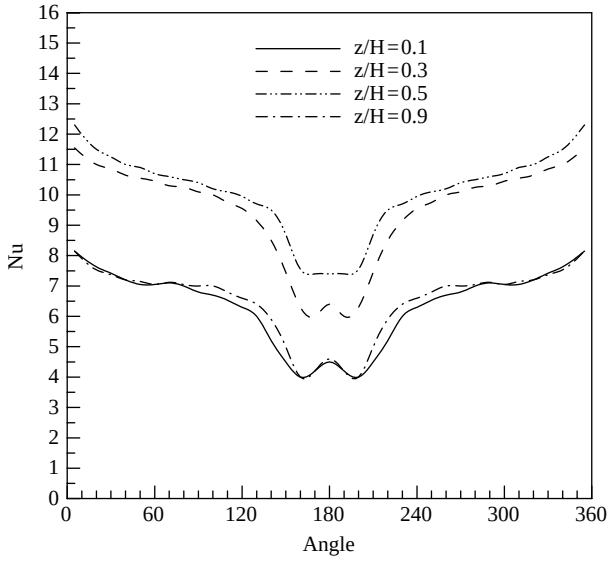

Figure 8.
Local Nusselt number around the tube at $t = 3$

the tube axis (Figure 8). Applying the symmetric boundary conditions, the above results were noticed.

Initially, the temperature gradients at the tube surface and also at the top and bottom walls were large. Moreover, the boundary layers were thin and the flow pattern was similar to that of the potential flow. Therefore, the Nusselt number was large and its variations around the tube and along the z-direction were small (Figure 7).

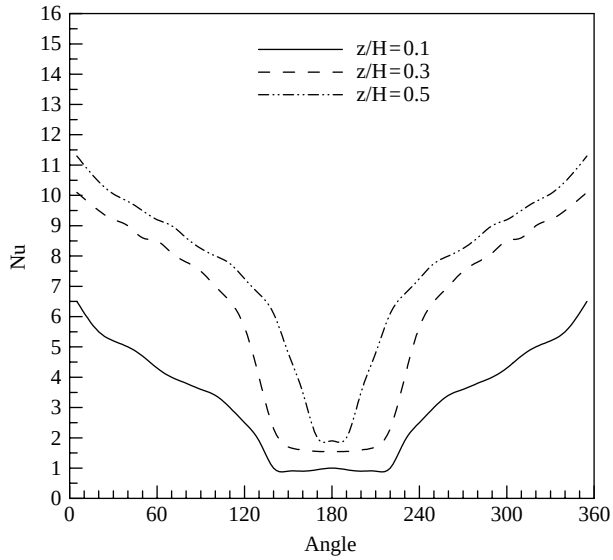

Figure 9.
Steady-state local Nusselt number around the tube

However, as time proceeds, the wake behind the tube grows in size; thus, the local Nusselt number decreases moving from the front ($\varphi = 0°$) to the back ($\varphi = 180°$) of the tube (Figures 8 and 9). It should be noted that similar observations were made by El-Shaboury and Ormiston (2005) and Chen *et al.* (1986) when conducting two-dimensional simulations of non-isothermal flow past over cylinders. At a fixed angle, the local Nusselt number decreases by moving in the z-direction towards the top and bottom walls. This decrease is due to the reduction of the velocities in the boundary layers near the walls. For a fixed value of z/H, the temperature gradient at the tube wall decreases and the thickness of the boundary layers increases as time proceeds. Therefore, the local Nusselt number approaches its minimum value which occurs at the steady-state condition. These observations are in agreement with the numerical results of Gowda *et al.* (1998) for an in-line tube bank.

Variations of the average Nusselt number with respect to z/H at two different times and for the steady-state condition are shown in Figure 10. It is observed from this figure that the largest average Nusselt number always occurs at the mid-plane, i.e. at $z/H = 0.5$.

4.4.1 Effects of the tube length. To examine the effects of the tube length on the results, computational domains with different values of H, namely, $H = 2D$, 3D, and 6D, are considered. Based on physical observations, the effects of the top and bottom walls on the flow field and, in turn, on the computed Nusselt number should decrease as the tube becomes longer. Eventually, for large enough values of the tube length, the two-dimensional results should be retrieved.

Figure 11 shows the variations of the steady-state local Nusselt number at the mid-plane, $z/H = 0.5$, with respect to the tube length. It is observed from the figure that the local Nusselt number decreases with increasing the tube length. This decrease, which is more significant in the front of the tube, is due to the decreasing velocities outside the boundary layer, and the reduction in the temperature gradients at the top and bottom walls.

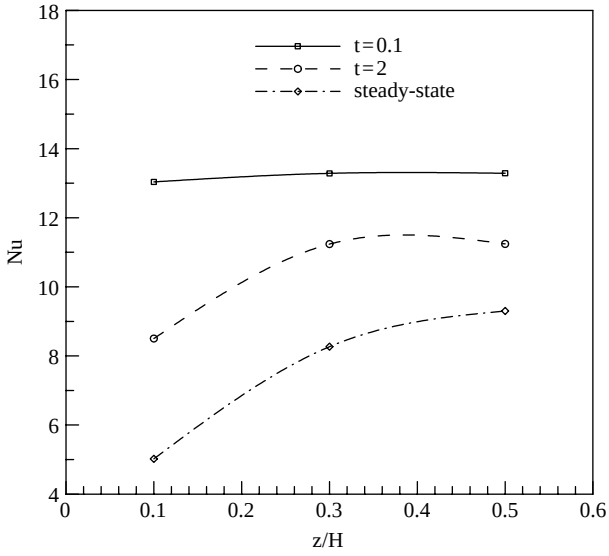

Figure 10.
Variation of the average Nusselt number with respect to z/H

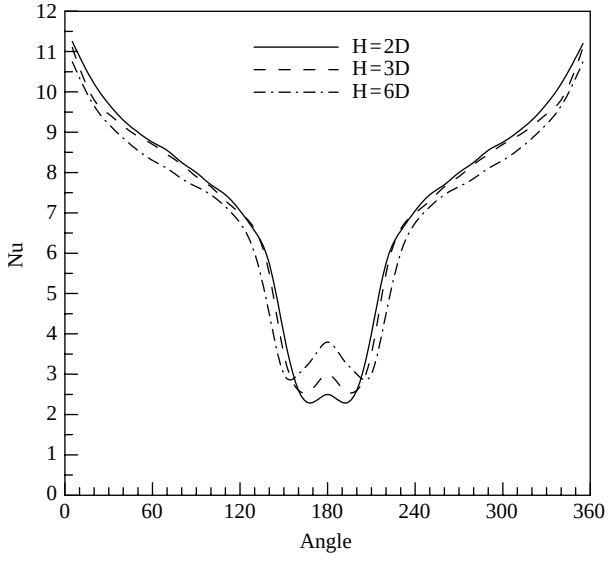

Figure 11.
Variation of the steady-state local Nusselt number with the tube length for z/H = 0.5

The variations of the steady-state average Nusselt number with respect to the tube length at the mid-plane is shown in Figure 12. It is clear from the figure that the average Nusselt number decreases with increasing the tube length. For H/D greater than six, the average Nusselt number converges to 7.1 which is the average Nusselt number for the two-dimensional case for $Re = 250$ and $Pr = 0.7$ (McAdams, 1954). Hence, demonstrating that for long tubes ($H \geq 6D$), two-dimensional results can be retrieved from the proposed three-dimensional scheme.

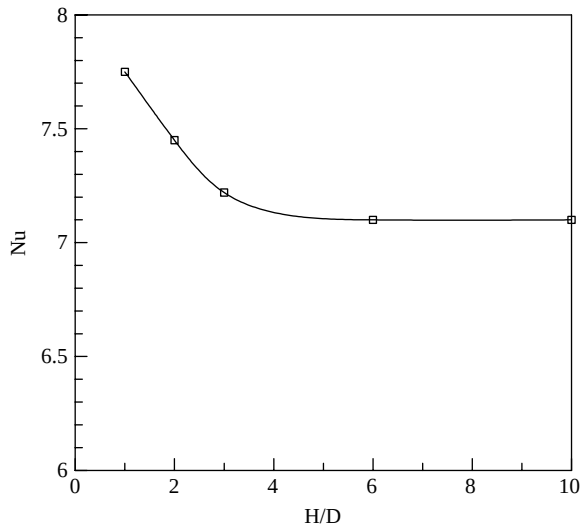

Figure 12.
Variation of the steady-state average Nusselt number with the tube length for $z/H = 0.5$

5. Concluding remarks

A hybrid finite difference-finite element method has been introduced and applied to solve the three-dimensional, transient energy equation for the non-isothermal fluid flow past over a tube in a channel. The proposed hybrid scheme employes a two-dimensional finite element method in the planes perpendicular to the tube axis; while, the derivatives along the tube axis are discretized using the finite difference technique. The Taylor-Galerkin method is used to obtain stable solutions for high Peclet numbers.

To assess the performance of the hybrid scheme, the method was implemented on some three-dimensional test cases. The L^2-norm of the error between the exact and the numerical solutions were calculated for three different hybrid meshes. The results show that the numerical solution converges to the exact solution with refining the mesh. To compare the computational time of the hybrid scheme with that of the three-dimensional finite element method, the three-dimensional finite element method was applied to one of the test cases for the same time step and nodes using the same computer. The results show that the computational time of the hybrid scheme is approximately one-third of that for the three-dimensional finite element method. The main reason for the lower computational time of the hybrid scheme is its lower nodal connectivity compared to the three-dimensional finite element method. This characteristic of the hybrid scheme is advantageous in the large-scale numerical simulations of three-dimensional problems where the computational time duration is an issue.

Subsequently, the method was employed to simulate numerically the three-dimensional heat transfer in the non-isothermal fluid flow passing over a circular tube in a channel for $Re = 250$, $Pr = 0.7$, $T_w = 400\,K$ and $T_\infty = 300\,K$. The flow field was solved using the three-dimensional finite element method. Having obtained the velocity field, the hybrid scheme was employed to solve the energy equation. In this respect, mesh independent studies were performed and the effects of the location of the outlet boundary on the results were investigated. Based on these

studies, the simulations were conducted for $L/D = 12$ using the mesh with 7,216 nodes for which the average and the local Nusselt numbers were calculated.

The results show that the Nusselt number decreases as φ increases from 0° to 180° and also by approaching the top and bottom walls. Furthermore, concerning the effects of the tube length on the average Nusselt number, the results show that the Nusselt number decreases with increasing the tube length, and for the tube length greater than six times of the tube diameter the average Nusselt number converges to the value for the two-dimensional case. In addition, the numerical experiments show that increasing the domain length beyond 12D has insignificant effects on the results.

Altough much arduous and lengthy work for other aspects of the proposed method implementation remain to be studied (on which some work are already being pursued), based on the results obtained, the introduced numerical method in this present study offers much ease for solving multi-dimensional problems specifically for those cases where fluid-flow and heat- transfer interconnection analysis produce complexity, for those cases involving too heavy nodal-bondings dependability, and of course, for those cases which substantional computational time duration is a major drawback.

References

Arefmanesh, A. and Afkhami, S. (2001), "A Taylor-Galerkin/control volume model for the simulation of heat transfer with phase change in a fluid flow", *ISME, Proceedings of 5th International and 9th Annual Mechanical Engineering Conference*, pp. 393-400.

Baer, T.A., Cairncross, R.A., Schunk, P.R., Rao, R.R. and Sackinger, P.A. (2000), "A finite element method for free surface flows of incompressible fluids in three dimensions Part II dynamic wetting lines", *International Journal for Numerical Methods in Fluids*, Vol. 33, pp. 405-27.

Brooks, A.N. and Hughes, T.J.R. (1982), "Streamline-upwind/Petrov-Galerkin formulations for convection dominated flows with particular emphasis on the incompressible Navier-Stokes equations", *Computer Methods in Applied Mechanics and Engineering*, Vol. 32, pp. 199-259.

Cairncross, R.A., Schunk, P.R., Baer, T.A., Rao, R.R. and Sackinger, P.A. (2000), "A finite element method for free surface flows of incompressible fluids in three dimensions Part I boundary fitted mesh motion", *International Journal for Numerical Methods in Fluids*, Vol. 33, pp. 375-403.

Chen, B.F. (1998), "Hybrid three-dimensional finite-difference and finite-element analysis of seismic wave induced fluid-structure interaction of a vertical cylinder", *Ocean Engineering*, Vol. 25, pp. 639-59.

Chen, C.K., Wong, K.L. and Cleaver, J.W. (1986), "Finite element solutions of laminar flow and heat transfer of air in a staggered and an in-line tube banks", *International Journal of Heat and Fluid Flow*, Vol. 7, pp. 291-300.

El-Shaboury, A.M.F. and Ormiston, S.J. (2005), "Analysis of laminar forced convection of air cross-flow in in-line tube banks with nonsquare arrangements", *Numerical Heat Transfer*, Vol. 48, pp. 99-126, Part-A.

Gowda, Y.T.K., Patnaik, B.S.V.P., Narayana, P.A.A. and Seetharamu, K.N. (1998), "Finite element simulation of transient laminar flow and heat transfer past an in-line tube banks", *International Journal of Heat and Fluid Flow*, Vol. 19, pp. 49-55.

Heinrish, J.C. and Pepper, D.W. (1999), *Intermediate Finite Element Method, Fluid Flow and Heat Transfer Applications*, Taylor and Francis, Philadelphia, PA.

Launder, B.E. and Massey, T.H. (1978), "The numerical prediction of viscous flow and heat transfer in tube banks", *ASME Transactions, Journal of Heat Transfer*, Vol. 100, pp. 565-71.

McAdams, W.H. (1954), *Heat Transmission*, 3rd ed., McGraw-Hill, New York, NY.

Mashayek, F. and Ashgriz, N. (1995), "A hybrid finite-element-volume-of-fluid method for simulating free surface flows and interfaces", *International Journal for Numerical Methods in Fluids*, Vol. 20, pp. 1363-80.

Morton, M.T.W. and Tony, W.H.S. (1997), "On a compact mixed-order finite element for solving the three-dimensional incompressible Navier-Stokes equations", *International Journal for Numerical Methods in Fluids*, Vol. 25, pp. 513-22.

Passoni, G., Alfonsi, G. and Galbiati, M. (2002), "Analysis of hybrid algorithms for the Navier-Stokes equations with respect to hydrodynamic stability theory", *International Journal for Numerical Methods in Fluids*, Vol. 38, pp. 1069-89.

Tezduyar, T.E. and Shih, R. (1991), "Numerical experiments on downstream boundary of flow past cylinders", *Journal of Engineering Mechanics*, Vol. 117, pp. 854-71.

Tiwari, S. and Biswas, G. (2003), "Numerical prediction of flow and heat transfer in a rectangular channel with a built-in circular tube", *Journal of Heat Transfer*, Vol. 125, pp. 413-21.

Usmani, A.S., Cross, J.T. and Lewis, R.W. (1992), "A finite element model for the simulations of mould filling in metal casting and the associated heat transfer", *International Journal for Numerical Methods in Engineering*, Vol. 35, pp. 787-806.

Wong, K.L. and Baker, A.J. (2002), "A 3D incompressible Navier-Stokes velocity-vorticity weak form finite element algorithm", *International Journal for Numerical Methods in Fluids*, Vol. 38, pp. 99-123.

Zhang, J. and Dalton, C. (1998), "A three-dimensional simulation of a steady approach flow past a circular cylinder at low Reynolds number", *International Journal for Numerical Methods in Fluids*, Vol. 26, pp. 1003-22.

Corresponding author
A. Arefmanesh can be contacted at: a_aref32@yahoo.com